[redacted]

Corrections for the hydrodynamic instability based critical heat flux models in pool boiling – effects of viscosity and heating surface size

Huayong Zhao[1*], Colin P. Garner[1]

1. Wolfson School of Mechanical, Electrical and Manufacturing Engineering

Loughborough University, Leicestershire, LE11 3TU, United Kingdom

* Corresponding author. H.Zhao2@lboro.ac.uk

Abstract

This paper presents corrections for existing hydrodynamic instability based Critical Heat Flux (CHF) models in pool boiling by taking into account the effect of the viscosity, geometry and size of the liquid-vapour interface. Based on the existing literature, the Kelvin – Helmholtz theory, used by the most commonly adopted CHF models, can lead to noticeable errors when predicting the instability conditions. The errors are mainly due to the inaccuracy of the inviscid flow assumptions and the oversimplification of the interface geometry. In addition, the literature suggests the most unstable condition predicted by the Viscous Correction for Viscous Potential Flow (VCVPF) theory for the cylindrical interfaces best match the observed air column breakup conditions in water. In this paper, the most unstable instability conditions predicted by the VCVPF theory are used to correct the existing CHF models. The comparison between the existing and corrected CHF models suggests that the corrected models always predict a higher CHF value. In addition, the corrected Zuber model predicts similar CHF value to the Lienhard and Dhir model. The comparison with experimental data suggests that the correction to the Zuber model can increase its prediction accuracy in most cases, but not necessary for the Lienhard and Dhir model. When compared to experimental CHF data for boiling cryogens at different pressures, the corrected CHF models are consistently more accurate than the original CHF models.

1. Introduction

Boiling has many important practical applications due to its effectiveness in dissipating excessive thermal load by taking advantages of the liquid-vapour phase change processes and the associated large latent heat. Among the different boiling conditions, the critical heat flux (CHF) point, where the heat transfer rate starts to reduce as the surface temperature increases, plays a crucial role in assuring the safety of the system. When the imposed heat flux is larger than CHF, the surface temperature rapidly increases to the so-called burnout temperature, which can be well above the softening point or even the melting point of the heating surface, causing potential system failure. Therefore, the ability to predict the CHF accurately in different operation conditions is vital for many practical applications.

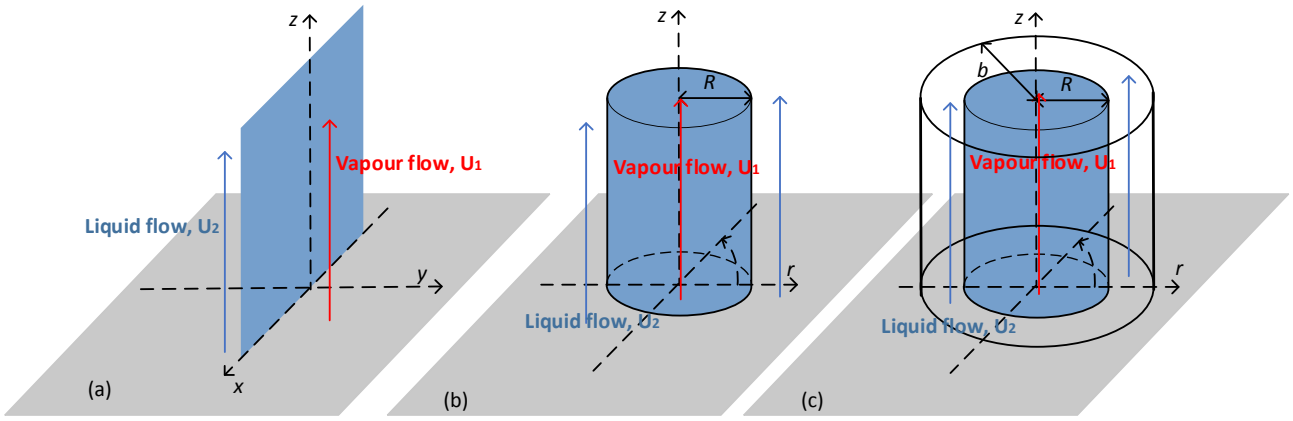

Fig. 1 The geometry of the undisturbed interface in (a) Kelvin-Helmholtz (KH) instability theory used in typical hydrodynamic CHF models, (b) hydrodynamic CHF models, (c) KH theory used on this paper to correct for the CHF models

Many different models have been proposed to predict the CHF, as summarized and compared to the experimental data by many researchers, e.g. [1–3]. Their results showed that the most accurate models were all containing elements from the analysis of the Kelvin-Helmholtz (KH) instability of a Planar interface between two separate Inviscid Potential Flows (PIPF) of infinite sizes, as in Fig. 1(a). However, the assumed liquid-vapour interface in most hydrodynamic CHF models was usually cylindrical and of finite size, as in Fig. 1 (b).

As a result, the negligence of the effects of viscosity, the inaccurate geometry, and the lack of size parameter in the PIPF analysis could introduce noticeable error in predicting the instability condition.

The existing theoretical and experimental analyses of the KH instability for interfaces of different geometry and in different flow conditions [4–7] have shown noticeable differences in the predicted unstable conditions when taking into account the effect of viscosity and the interface geometry. Therefore, all the existing CHF models based on the PIPF-KH theory need to be corrected to capture the physics more accurately.

In this paper, the existing PIPF-KH theory based CHF models will be reviewed first in Section 2.1. Then, the effect of viscosity and system geometry on the KH theory will be briefly reviewed in Section 2.2. In Section 3, the corrected CHF models will be presented. Finally, the comparison between the results of existing CHF models, the corrected models and the experimental data will be presented in Section 4 to show the difference.

2. Review of the existing CHF and KH models

2.1 Existing CHF models

The existing models used to predict the CHF in pool boiling can be grouped into four different types: (i) the hydrodynamic instability models, (ii) the hydrodynamic force imbalance model, (iii) the macrolayer dryout models, and (iv) the Irreversible dry Hot Spots (IHS) models. The formulae and the assumptions related to the KH instability underlying these models will be reviewed here. Discussion on the other hypothesis and assumptions and a few other types of models which do not build on the KH instability have been summarized in the established literature [1–3].

(i) The hydrodynamic instability models

The precursor of the hydrodynamic instability models was first introduced in 1950 by Kutateladze [8] through non-dimensional analysis. The link between the Kutateladze model and the hydrodynamic instability was then identified by Zuber [9], and his model became the base model in this group. Zuber postulated that the CHF occurred when the vapour flow velocity reached the critical value predicted by the PIPF-KH theory, and then the vapour columns broke up to block the effective vapour transport routes. Lienhard and Dhir [10] modified Zuber's model and extended it to different configurations, such as for small heating surface, cylindrical and spherical heating surfaces, as reviewed by Carey [3]. In addition, many other empirical coefficients have been introduced by different researchers to correct Zuber model when using different fluids, system configurations, and surfaces with different wettabilities, via curve fitting to the experimental data [11][12].

The key assumptions behind all these models related to the KH instability were:

1. The vapour columns were assumed to be cylindrical, as in Fig. 1 (b), and distributed in a rectangular array predicted by the two-dimensional Rayleigh-Taylor (RT) instability theory. Zuber [9] used the critical wavelength ($\lambda_{C,RT}$) and the most dangerous wavelength ($\lambda_{D,RT} = \sqrt{3}\lambda_{C,RT}$) predicted by the RT theory as the separation distance to calculate the upper and lower limits of the CHF. Lienhard and Dhir [10] used the most dangerous wavelength. The radius of the vapour column (R) in both models was assumed to be equal to one quarter of the instability wavelength.
2. The KH unstable wavelength (λ_{KH}) imposed on the columns in Zuber's model was assumed to be equal to the Plateau-Rayleigh (PR) instability wavelength for circular jets ($\lambda_{KH,Z} = 2\pi R$). λ_{KH} in the Lienhard and Dhir model was assumed to be equal to the most dangerous wavelength in RT instability ($\lambda_{KH,LD} = \lambda_{D,RT} = \sqrt{3}\lambda_{c,RT}$).

The critical relative velocity (V_c) between the liquid phase and the vapour phase can then be calculated by the PIPF-KH theory:

$$V_{c-PIPF} = |\bar{V}_l - \bar{V}_v| = \left[\frac{2\pi\sigma(\rho_l+\rho_v)}{\rho_l\rho_v\lambda_{KH}}\right]^{1/2} \quad (1)$$

Since $\rho_l \gg \rho_v$, to satisfy the continuity equation, $V_{c-PIPF} \cong V_v \cong \left[\frac{2\pi\sigma}{\rho_v\lambda_{KH}}\right]^{1/2}$. The PIPF-KH theory is derived by assuming infinite depth in both phases, so there is no size parameter in Eq. (1).

The CHF is then calculated by assuming all the heat is used to evaporate the liquid so it can be calculated by

$$q''_{CHF} = \rho_v V_{c-PIPF} h_{lv} \left(\frac{A_v}{A_s}\right) = \rho_v h_{lv} (\frac{\pi}{16}) \left[\frac{2\pi\sigma}{\rho_v\lambda_{KH}}\right]^{1/2} \quad (2)$$

The RH instability analysis (KH instability for a horizontal surface with negligible interface velocity: $V_l = V_v = 0$) suggests:

$$\lambda_{C,RT} = 2\pi \left[\frac{\sigma}{(\rho_l-\rho_v)g}\right]^{1/2}; \lambda_{D,RT} = \sqrt{3} \cdot \lambda_{C,RT} \quad (3)$$

The arithmetic mean of the upper limit (i.e. $\lambda_{KH} = \lambda_{C,RT}$) and the lower limit (i.e. $\lambda_{KH} = \lambda_{D,RT}$) can be calculated by [9]:

$$q''_{CHF,Z} = \frac{(q''_{CHF,Z,upper}+q''_{CHF,Z,lower})}{2} = 0.138\rho_v h_{lv} \left[\frac{\sigma(\rho_l-\rho_v)g}{\rho_v^2}\right]^{1/4} \quad (4a)$$

Zuber also introduced a simpler way to get the average value, which was using $\lambda_{C,RT}$ as the instability wavelength but scaled down the coefficient [9]. The result is Eq. (4b) and was widely adopted as the Zuber model in the literature to calculate the CHF.

$$q''_{CHF,Z} = 0.131\rho_v h_{lv} \left[\frac{\sigma(\rho_l-\rho_v)g}{\rho_v^2}\right]^{1/4} \quad (4b)$$

Lienhard and Dhir model [10] can be written as a function of Zuber model such that: $q''_{CHF,LD} = 1.14 q''_{CHF,Z}$.

The KH instability wavelength used in both models was not from the proper KH instability analysis but from either the PR instability or the RT instability analysis. However, both RT and PR instability conditions are different from the flow conditions in boiling. The sizes of the vapour columns used in these two models also could not be fully justified. Despite these difficulties, the analytical models developed by Zuber, and Lienhard and Dhir are able to predict the CHF in many saturated pool boiling conditions on smooth surfaces to within approximately ±20% accuracy [3]. The comparison done by Fang and Dong showed that the most accurate models used to predict CHF conditions were those empirical correlations modified from the Zuber model [1]. This suggests that the existing analytical hydrodynamic instability models are likely to be incomplete models and should be revised to predict the experimental observations better.

(ii) Hydrodynamic force imbalance model

Kandlikar developed a model based on the hydrodynamic behaviour of a single detached bubble to predict the q''_{CHF} [13]. He hypothesised that the CHF occurred when the repulsive force, coming from the liquid evaporation on the interface, surpassed the surface tension forces and the gravitational forces normal to the liquid-vapour interface. Consequentially, the bubble was stretched sideways to merge with the adjacent bubble to form a vapour blanket which covered part or the whole heating surface. Kandlikar assumed the average bubble size could be taken as $\lambda_{C,RT}/2$, and the correlation can be represented as in Eq. (5) [13].

$$q''_{CHF,K} = h_{lv} \cdot \rho_v \cdot \left[\frac{\sigma g(\rho_l - \rho_v)}{\rho_v^2}\right]^{1/4} \cdot \frac{1+\cos\beta}{16} \cdot \left[\frac{2}{\pi} + \frac{\pi}{4}(1 + cos\beta)cos\phi\right]^{1/2} \quad (5)$$

Comparison with the experimental data [1] [13] indicated that the Kandlikar model could predict the q''_{CHF} within 30% uncertainty for various fluids when the contact angle ranged from 0° to 90°. Although the measurement of the dynamic receding contact angle in practice requires some efforts, the implementation of the model after knowing the dynamic contact angle is straightforward. Therefore, this model can be used to provide the baseline predictions for a wide range of fluids and operation conditions. However, there is no justification of why the average bubble diameter is half the critical RT instability wavelength.

(iii) Macrolayer dryout models

The macrolayer dryout model was initially proposed by Haramura and Katto [14]. This group of models assumed that large bubbles were hovering above a macrolayer which consists of numerous small vapour jets dispersed inside the thin liquid film. The evaporation of the liquid film in this layer fed the vapour to the large bubbles above them. The model assumed that CHF occurred when this macrolayer was evaporated completely before the bubble grew large enough to escape from the surface. Therefore, the q''_{CHF} can be calculated as the total amount of heat required to evaporate all the liquid films inside the macrolayer.

This group of models assumed:

1. The macrolayer layer thickness (δ) must be proportional to the KH instability wavelength (λ_{KH}). The original model assumed $\delta = \lambda_{KH}/4$.
2. The intervals between bubbles were the most dangerous wavelength ($\lambda_{D,RT}$) predicted by the RT instability.

The q''_{CHF} can then be calculated as [14]:

$$q''_{CHF,HK} = q''_{CHF,Z}\left(\frac{\pi^4}{2^{11}.3^2}\right)^{1/16}\left(\frac{A_v}{A_s}\right)^{5/8}\left(1-\frac{A_v}{A_s}\right)\left\{\frac{(\rho_l/\rho_v)-1}{\left((11/16)(\rho_l/\rho_v)+1\right)^{3/5}}\right\}^{5/16} \quad (6)$$

The Haramura and Katto model was in good agreement with Zuber's model when $A_v/A_s = 0.584(\rho_v/\rho_l)^{0.2}$ [14]. The Haramura and Katto model has been revised by many researchers based on the different hovering period and macrolayer thickness models to fit the experimental data better, as detailed in ref. [1].

(iv) Irreversible dry Hot Spots (IHS) models

The hydrodynamic instability based IHS model was newly introduced by Zhao and Williams based on some of the latest experimental observation of the critical heat flux conditions [2]. This model was based on the experimental observations that CHF occurred when there were IHS which were triggered by consistent instability-induced bubble 'necking' and separation processes [15–17]. These IHS grew with time due to the significantly increased surface temperature nearby and eventually permanently covered a large part of the surface to trigger the CHF. The model assumed that the bubble 'necking' process was triggered by the KH instability. Assuming the sensible heat was negligible, the base equation of the model can be represented by:

$$\frac{\bar{q}''_{CHF,IHS}}{\bar{q}''_{w,c}} = C \in \left[1, \sqrt{3/2}\right], q''_{w,c} = \sqrt{\frac{2\pi\sigma(\rho_l+\rho_v)}{\rho_l\rho_v h_{neck}}}\,\rho_v h_{fg}\frac{A_{neck}}{A_{base}} \quad (7)$$

$C = 1$ corresponds to the critical velocity predicted by the PIPF-KH theory, and $C = \sqrt{3/2}$ corresponds to the most unstable velocity predicted by the PIPF-KH theory (i.e. where the interface perturbation grows at the maximum rate). Comparison to the experimental visualization data reported in literature suggested C was close to 1.1, which was approximately the mean value of the upper and lower limit [2].

The height of the 'necking' position (h_{neck}) was taken as the KH instability wavelength since only the perturbation with dominant wavelength equals to h_{neck} would most likely cause the break up at this position.

When the heater size is larger than the most dangerous wavelength predicted by the RT instability (i.e. $\lambda_{D,RT}$ in Eq. (3)), the bubble base area will be ultimately limited by the RT instability so $A_{base} = \pi \cdot \lambda_{D,RT}^2/4$. When the heater size is smaller than $\lambda_{D,RT}$, the actual heater area is used.

The value of h_{neck}, A_{neck} were based on the analysis of a simplified bubble nucleation and merging process, as illustrated in Fig. 2.

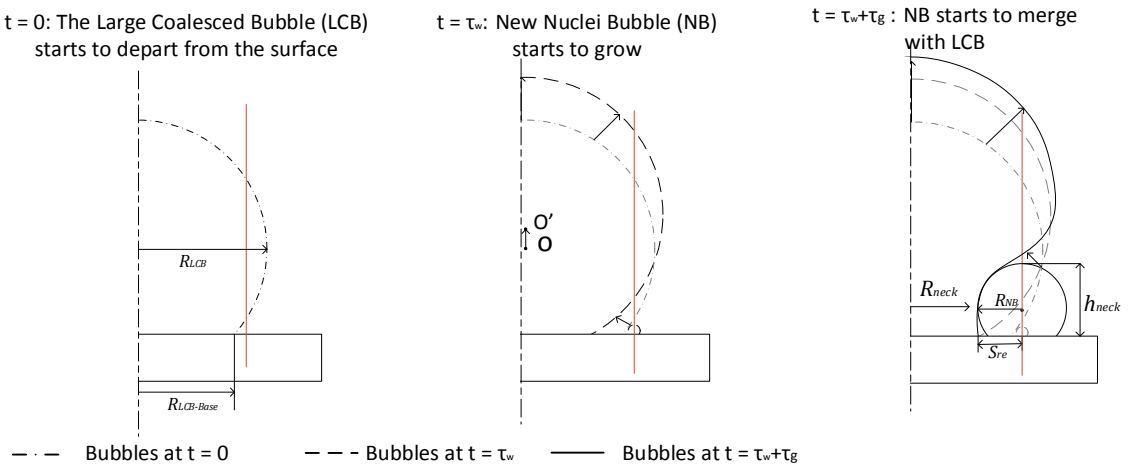

Fig. 2 Cross-sectional view of the threshold condition for the bubble merging (spatial and temporal averaged behaviour) [2]

The bubble necking occurs when the vapour flow velocity in the neck position and the h_{neck} satisfy the KH instability criteria at $t = \tau_w + \tau_g$, i.e. when the bubbles start to merge so that more vapour is fed to the neck position. Therefore, the height and the radius of the neck can be calculated by Eq. (8):

$$h_{neck}(\tau_g) = R_{NB}(\tau_g) \cdot (1 + \cos\beta_{re});$$

$$R_{neck}(\tau_g) = R_{LCB,base}(\tau_g) \tag{8}$$

R_{NB} is calculated by the existing bubble growth models which all share the same form of the formula, as follows:

$$R_{NB}(\tau_g) = \gamma \cdot (\alpha_l \tau_g)^n; \gamma = C_1 \cdot Ja;\ Ja = \frac{\Delta T_s \cdot C_{p,l} \cdot \rho_l}{h_{lv} \cdot \rho_v}; \Delta T_s = T_s - T_{sat} \tag{9}$$

As reviewed by Zhao and Williams [2], n was reported to be equal to 0.5 in most models and experiments. The bubble growth coefficient C_1 was found between 1.4 and 1.7 for the horizontal surface at atmospheric pressure. The fitting of the IHS to the experimental data reported by Bailey *et al.* [18] suggested a simple linear correlation between C_1 and pressure (in unit of bar):

$$C_1 = 1.21 \cdot P + 0.19; \quad (10)$$

The excess surface temperature was calculated based on the established nucleation boiling correlation, such as the one suggested by Rohsenow [19], i.e. Eq. (11).

$$\Delta T_s = \left[\left(\frac{q_s''}{\mu h_{lv}}\right) \cdot \left(g \cdot \frac{\rho_l - \rho_v}{\sigma}\right)^{-0.5}\right]^{\frac{1}{3}} \cdot \frac{C_{sf} \cdot h_{lv} \cdot Pr_l^m}{C_{P,l}} \quad (11)$$

Since ΔT_s is proportional to $q_s''^{1/3}$ so it will not be sensitive to the small change of q_s''. The coefficients C_{sf} and m depend on the combination of fluids and surface and has been well documented in the literature , e.g. [3].

R_{base} was calculated by considering the force balance on the Large Coalesced Bubble (LCB) between the inertial force due to bubble growth and buoyancy. Based on the experimental observation that the maximum LCB size was close to the critical wavelength in RT instability (i.e. $\lambda_{c,RT}$) at different pressure [20], the formula for R_{base} was derived as [2]:

$$R_{LCB,base}(t) = \left(\gamma_{LCB}^2 \cdot (\alpha_l t)^{2n} - \left(\frac{g}{3n+1}\right)^2 t^4\right)^{0.5}; \gamma_{LCB} = \left(\frac{(\lambda c,_{RT}/2)^{(2-n)/n} \cdot g}{(3n+1) \cdot \alpha_l^2}\right)^{\frac{n}{2}}; \quad (12)$$

Based on the experimental observation that the superheated layer thickness in saturated water pool boiling conditions was consistent to be ~ 1 mm [21]. The Nuclei Bubble (NB) is assumed to start to grow in the position where the microlayer underneath the LCB is 1 mm. The characteristic waiting time for bubble nucleation (τ_w) can be calculated based on the bubble inception condition described by Davis and Anderson [22], and its formula has been

derived by Zhao and Williams [2]. In saturated boiling condition, Zhao and Williams showed that $\tau_w \ll \tau_g$ so can be ignored.

Equation (7) – (12) can then be solved simultaneously by applying the bubble merging condition observed by Chu *et al.* [17]: $R_{NB}(\tau_g) = S_{re}(\tau_w + \tau_g)$, where S_{re} is the distance between the nucleation sites and the bubble base. There are multiple solutions to this equation sets since the heat flux larger than CHF can still satisfy the criteria described by Eq. (7). Therefore, the CHF condition is corresponding to the solution with the lowest heat flux value.

The IHS model couples the observed bubbling process with the KH instability and takes into account the effect of wettability and the heater size. Although the IHS model was based on the simplified bubble nucleation and merging process and several established semi-empirical correlations, it has been shown to be able to trace the effect of heater size and geometry (i.e. horizontal flat surface and horizontal cylinders), the surface wettability (both hydrophobic and hydrophilic surface), and the pressure much better than all the other existing CHF models [2]. In addition, the predicted detailed bubble grow and merge process were found in good agreement with the experimental results reported in the literature [2].

In summary, all these four different types of CHF models are based on the critical condition predicted by the PIPF-KH theory (i.e. the condition where the interface perturbation will start to grow with time). Theoretical analysis and experimental observations showed that the PIPF-KH theory could lead to large errors in predicting the actual instability conditions [7].

2.2 KH instability theories

The KH instability occurs when two fluids separated by a well-defined interface flow at different velocities. The simplest form of the KH instability is based on a planar interface between two inviscid fluids with infinite depth, i.e. the PIPF-KH theory. The critical condition when any perturbation of the interface starts to grow with time can be predicted by the

PIPF-KH theory as in Eq. (1). The most unstable condition occurs when the perturbation of a known wavelength grows at the highest rate. It has been shown by Zhao and Williams that $V_{D-PIPF} = \sqrt{3/2} \cdot V_{c-PIPF}$ [2].

However, in practical boiling systems, the liquid-vapour interface is closer to a cylindrical shape, as in Fig. 1 (b), and both the vapour columns and the space between vapour columns are of limited sizes. In addition, although the vapour phase has a very small viscosity, the liquid phase can have high enough viscosity to affect the instability. The assumptions and formulations of three different KH theories which applied to the cylindrical interface will be briefly reviewed in this session. A detailed review of the assumptions and formulations on different types of KH theories can be found elsewhere [7,23].

The corrections for the finite size has been tackled by Lee [24]. The formulation of a cylindrical vapour column with finite size and with negligible interfacial heat and mass transfer, as in Fig. 1(c), has been given by Zhao and Bhabra [7] and is named Inviscid Potential Flow (IPF) KH theory on this paper. The perturbation growth rate ($w = w_r + iw_i$) can be calculated using the following equation:

$$a_0 w^2 + a_1 w + a_2 = 0 \tag{13}$$

$$a_0 = \rho_2 E_{1R} - \rho_1 F_{1R}; a_1 = 2k(U_1 \rho_1 F_{1R} - U_2 \rho_2 E_{1R});$$

$$a_2 = k^2(U_2^2 \rho_2 E_{1R} - U_1^2 \rho_1 F_{1R}) + \frac{k\sigma}{R^2}(k^2 R^2 - 1 + m^2);$$

$$E_{1R} = E_1(kR); F_{1R} = F_1(kR); E_1(kr) = \frac{I_m(kr)K'_m(kb) - K_m(kr)I'_m(kb)}{I'_m(kR)K'_m(kb) - I'_m(kb)K'_m(kR)}; F_1(kr) = \frac{I_m(kr)}{I'_m(kR)}$$

The critical condition can then be found when $w_i = 0$:

$$V_{c-IPF}^2 = (U_1 - U_2)^2 = \frac{\sigma}{kR^2}(1 - k^2 R^2 - m^2) \cdot \frac{\rho_1 F_{1R} - \rho_2 E_{1R}}{\rho_1 \rho_2 E_{1R} F_{1R}} \tag{14}$$

The most unstable condition (i.e. V_{D-IPF}) can be found by finding the maximum value of w_i using Eq. (13) when different values of perturbation wavenumber (k) are used. Equation (13) is too difficult to solve analytically to get the explicit solutions so it will be calculated numerically.

The correction for the effect of viscosity was first carried out by Funada and Joseph [25] through the approach they called Viscous Potential Flow (VPF) analysis. Their analysis takes into account the normal component of the viscous stress without violating the assumption of the irrotational flow. This approach has been taken by Awasthi and Agrawal [26] to analyse the cylindrical liquid-vapour interface in flow conditions around a solid cylindrical fuel rod. The formulation they derived has been modified based on the difference in boundary conditions by Zhao and Bhabra [7] for the vapour column illustrated in Fig. 1 (c), i.e.

$$a_0 w^2 + (a_1 + ib_1)w + (a_2 + ib_2) = 0 \quad (15)$$

$$a_0 = \rho_2 E_{1R} - \rho_1 F_{1R}; a_1 = 2k(U_1 \rho_1 F_{1R} - U_2 \rho_2 E_{1R});$$

$$b_1 = 2k^2(\mu_2 E_{2R} - \mu_1 F_{2R}); a_2 = k^2(U_2^2 \rho_2 E_{1R} - U_1^2 \rho_1 F_{1R}) + \frac{k\sigma}{R^2}(k^2R^2 - 1 + m^2);$$

$$b_2 = 2k^3(\mu_1 U_1 F_{2R} - \mu_2 U_2 E_{2R});$$

$$E_{2R} = E_{1\mathrm{R}}\left(1 + \frac{m^2}{k^2R^2}\right) - \frac{1}{kR}; F_{2R} = F_{1\mathrm{R}}\left(1 + \frac{m^2}{k^2R^2}\right) - \frac{1}{kR}$$

The critical condition in the VPF-KH theory can be calculated by using the expression:

$$V_{c-VPF}^2 = (U_1 - U_2)^2 = \frac{[\sigma k(k^2R^2 + m^2 - 1)/R^2] \cdot [2k^2(\mu_1 F_{2R} - \mu_2 E_{2R})]^2}{4k^6(\rho_1 \mu_2^2 F_{1R} E_{2R}^2 - \rho_2 \mu_1^2 E_{1R} F_{2R}^2)} \quad (16)$$

The most unstable condition (i.e. V_{D-VPF}) can again be obtained by solving Eq. (15) numerically.

Further correction for the tangential shear viscous stress has been done by Joseph and Wang [5] through a new approach named Viscous Correction of the Viscous Potential Flow analysis (VCVPF). They introduce a viscous pressure term to resolve the discrepancy between the zero-shear-stress boundary condition at a free surface and the non-zero irrotational shear stress. The comparison carried out by Wang *et al.* has shown that the VCVPF are in remarkably good agreement with the exact full viscous flow solution [27]. This approach has been taken by Awasthi *et al.* [23] to analyse the flows around a solid cylindrical fuel rod, and their formulation was modified by Zhao and Bhabra [7] for the cylindrical vapour column.

$$a_0 w^2 + (a_1 + ib_1)w + (a_2 + ib_2) = 0 \quad (17)$$

$a_0 = \rho_2 E_{1R} - \rho_1 F_{1R}; a_1 = 2k(U_1\rho_1 F_{1R} - U_2\rho_2 E_{1R});$

$b_1 = 2k^2[\mu_2 E_{3R} - \mu_1 F_{3R}]; a_2 = k^2(U_2^2\rho_2 E_{1R} - U_1^2\rho_1 F_{1R}) + \frac{k\sigma}{R^2}(k^2R^2 - 1 + m^2);$

$b_2 = 2k^3[\mu_1 U_1 F_{3R} - \mu_2 U_2 E_{3R}]; E_{3R} = E_{1R} + E_{2R}; F_{3R} = F_{1R} + F_{2R}$

The critical condition in the VPF-KH theory can be calculated by:

$$V_{c-VCVPF}^2 = (U_1 - U_2)^2 = \frac{[\sigma k(k^2R^2+m^2-1)/R^2]\cdot[2k^2(\mu_1 F_{3R}-\mu_2 E_{3R})]^2}{4k^6(\rho_1\mu_2^2 F_{1R}E_{3R}^2-\rho_2\mu_1^2 E_{1R}F_{3R}^2)} \quad (18)$$

In a similar manner to the VPF analysis, $V_{D-VCVPF}$ can be calculated by solving Eq. (17) numerically.

The comparison of the KH theories developed using the PIPF, IPF, VPF and VCVPF by Zhao and Bhabra [7] showed that the PIPF always overestimated the required relative velocity for the critical instability condition, especially when the instability wavelength was big. They also found that the PIPF theory could predict the most unstable condition accurately when the vapour column had radius >10 mm, and when the water chamber had radius >15 mm. In addition, their analysis showed the symmetry of the perturbation had a

negligible effect on the most unstable condition. Furthermore, they compared the theoretical predictions with the experimental data collected from a gas blowing rig and found that most of the gas columns broke up at the most unstable condition predicted by the VCVPF-KH theory. Considering the perturbation in the critical condition neither grows or attenuates while it grows at the highest rate in the most unstable condition, it is understandable that the most unstable condition is much more closed to the actual break up condition. Therefore, instead of using the critical condition predicted by the PIPF-KH theory as in existing CHF models, the most unstable condition predicted by the VCVPF-KH theory will be implemented to correct for the CHF prediction.

3. Corrected CHF models based on VCVPF-KH theory

All different hydrodynamic CHF models, including the Zuber model, and Lienhard and Dhir mode are based on the Eq. (2). Without changing the assumptions on the vapour column sizes and distributions, the model is revised by modifying the relative velocity terms. The corrected Zuber's model can be written as:

$$q''_{CHF,z'} = q''_{CHF,z} \cdot \frac{V_{D-VCVPF}}{V_{C-PIPF}} \text{ when } \lambda_{KH} = \frac{\pi}{2} \cdot \lambda_{C,RT} \quad (19)$$

The corrected Lienhard and Dhir model is:

$$q''_{CHF,LD'} = q''_{CHF,LD} \cdot \frac{V_{D-VCVPF}}{V_{c-PIPF}} \text{ when } \lambda_{KH} = \lambda_{D,RT} \quad (20)$$

As reviewed in session 2, the Haramura and Katto macrolayer dryout model, although built upon a different physical process, can be calculated by the same equation as the Zuber model due to the specific assumption of area ratio, so it will be represented by the corrected Zuber model in Eq. (19). The Kandlikar hydrodynamic forces imbalance model does not rely on the KH instability to calculate the CHF, so it remains unchanged.

The IHS is based on the Eq. (7), which can then be corrected as:

$$\bar{q}''_{CHF,IHS'} = V_{D,VCVPF} \cdot \rho_v h_{fg} \frac{A_{neck}}{A_{base}} \text{ when } \lambda_{KH} = h_{neck} \quad (21)$$

The corrected CHF value can be calculated by solving Eq. (21) together with Eq. (8) – (12) and Eq. (15) simultaneously.

4. Results and discussions

In this session, the comparison of the instability conditions predicted by different theories will be presented first. Then, the calculated CHF values from the existing models and the corrected models will be compared to the experimental data collected from different pool boiling conditions. The experimental data source and the related system configurations and conditions are summarized in Table 1.

Table 1. Summary of the experimental data source and related system conditions

Author	Surface/fluids	Pressure (bar)	Chamber size	A_{surf} (cm^2)
Bailey et al. [18]	Nickel coated copper / water, methanol	Water: 0.2 - 3 Methanol: 0.2 - 5	N/A, diagram shows >> the heating surface	1 x 1
Lienhard et al. [28]	Copper/Methanol Copper/Distilled water	Methanol: 0.446 - 0.981 Water: 0.145 - 0.427	Disc heater: 6.35 cm in radius Square heater: 2.16 - 0.89 cm in width	6.35 in radius; Square: 2.16, 1.84, 1.52, 1.21, 0.89
Bewilogua et al. [29]	Copper/He, H2, N2	0.03 < p/pc < 0.9	N/A, diagram shows >> the heating surface	N2: 2.9 H2 & He: 4.9

4.1 Comparison of the instability conditions predicted by different KH models

The comparison of the instability conditions for the interface between the saturated liquid water and water vapour at 1 bar pressure predicted by different KH models is shown in Fig. 3. It can be clearly seen from Fig. 3 that the PIPF theory overestimates the required relative velocity at the critical condition but can predict the required relative velocity at the most unstable condition accurately when the instability wavelength is less than 15 mm. It also shows the viscosity contributes to stabilize the interface by reducing the instability growth rate. These results indicate that, when compared to the existing CHF models which based

on the PIPF critical condition (i.e. Eq.(2)), the viscosity and size-corrected CHF models based on the critical instability condition will predict a lower CHF value since the CHF value is proportional to the velocity, while the corrected CHF based on the most unstable condition will predict a higher CHF value.

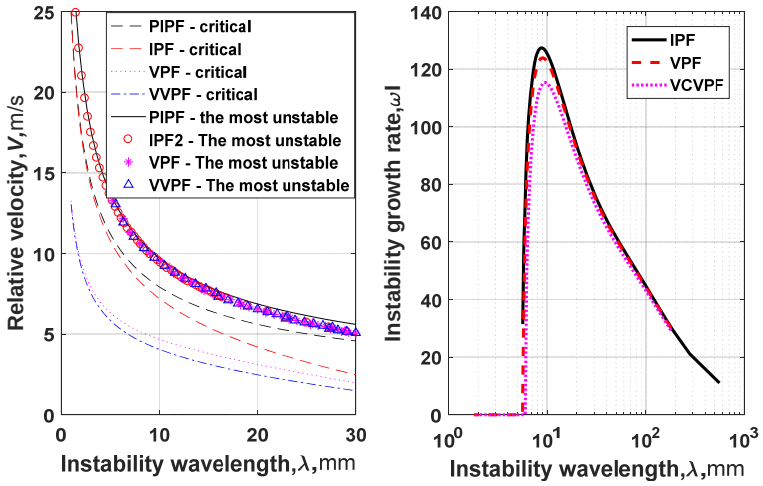

Fig. 3 The required relative velocity and instability growth rate at the critical condition and the most unstable condition for saturated water vapour column. $R = \lambda_{D,RT}/4$, $b = \lambda_{D,RT}/2$ at 1 bar system pressure, $m = 0$ (axisymmetric perturbation).

4.2 Effect of heater size on the CHF

The effect of the heater size on CHF has been experimentally investigated by Lienhard et al. [28], and they also suggested corrections for the original Lienhard and Dhir model by using the actual heater area, as in Eq. (22). The corrections applied to the Lienhard and Dhir model can also be applied to correct the Eq. (22).

$$\frac{q''_{CHF,L}}{q''_{CHF,Z}} = 1.14 \cdot \frac{\lambda^2_{RT,D}}{A_{heater}} \text{ when } \frac{L}{\lambda_{RT,D}} < \sqrt{2} \tag{22a}$$

$$\frac{q''_{CHF,L'}}{q''_{CHF,Z}} = 1.14 \cdot \frac{\lambda^2_{RT,D}}{A_{heater}} \cdot \frac{V_{D,VCVPF}}{V_{C,PIPF}} \text{ when } \frac{L}{\lambda_{RT,D}} < \sqrt{2} \text{ and } \lambda_{KH} = \lambda_{D,RT} \tag{22b}$$

Zhao and Williams have compared the results predicted by Eq. (22) with other existing CHF models [2]. A similar comparison together with the corrected CHF models and the experimental data is shown in Fig. 4. It shows that the corrected CHF models always predict a higher CHF because the required vapour velocity at the most unstable condition

predicted by the VCVPF-KH theory is higher than the velocity at the critical condition predicted by the PIPF-KH theory. In addition, it shows that Eq. (22) overestimates the CHF significantly when the heater is small. The corrected IHS model can predict the effect of heater size most accurately (~ 10% error on average), which is marginally better than the original IHS model.

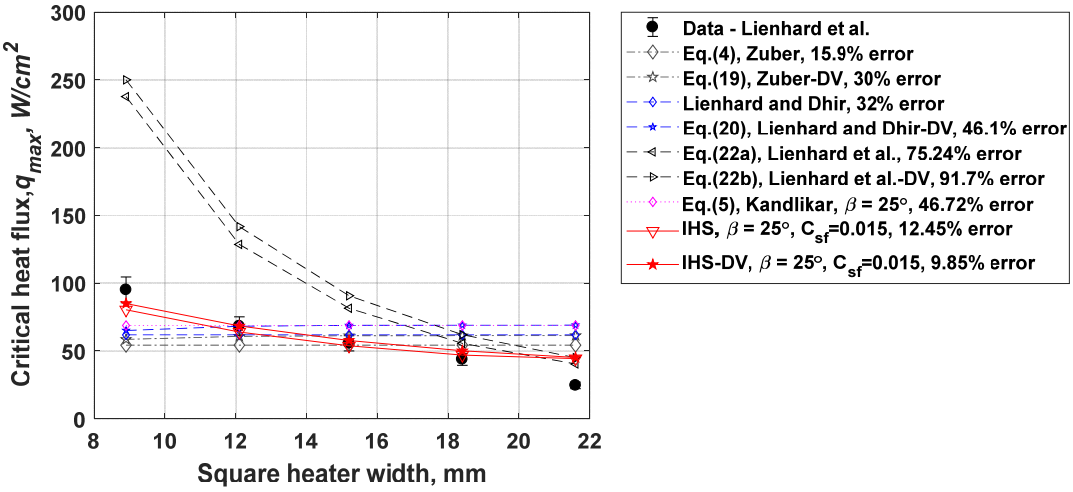

Fig. 4 The effect of heater size on the critical heat flux when boiling methanol at 1 bar pressure. $\lambda_{D,RT} = 17.4$ mm. The error bars represent ±10% error, percentage values on the legends are the average errors in predictions, and legends with "-DV" are corrected CHF models

4.3 The effect of system pressure on CHF

The effect of system pressure on CHF when boiling different fluids has been investigated experimentally by many researchers. In this session, all the contact angle values are taken from the literature documenting the original CHF models. The justification of the contact angle values can be found from the original literature.

Figure 5 shows the CHF results measured by Bailey *et al.* [18] and Lienhard *et al.* [28] when boiling water on the horizontal surface. It shows that the corrected IHS model with 35° contact angle, the corrected Zuber model and the original Lienhard and Dhir model fit the data collected by Bailey et al. best (< 5% error on average). The Kandlikar model with 85° contact angle fits the data collected by Lienhard *et al.* best. The contact angle was not

reported by the authors. Based on the work done by Horsthemke and Schrijder [30], the contact angle between water and freshly cleaned copper and nickel surface was less than 20° and the contact angle gradually increased to 40° after 4.5 hours exposure to oil-saturated air due to surface contamination, which was much smaller than the value used by the best fit Kandlikar model. The original IHS model incorporates a linear empirical correlation (i.e. Eq. 10) between the bubble growth rates and pressures based on the experimental data shown in the top plot in Fig. 5, so the good fit is no surprise.

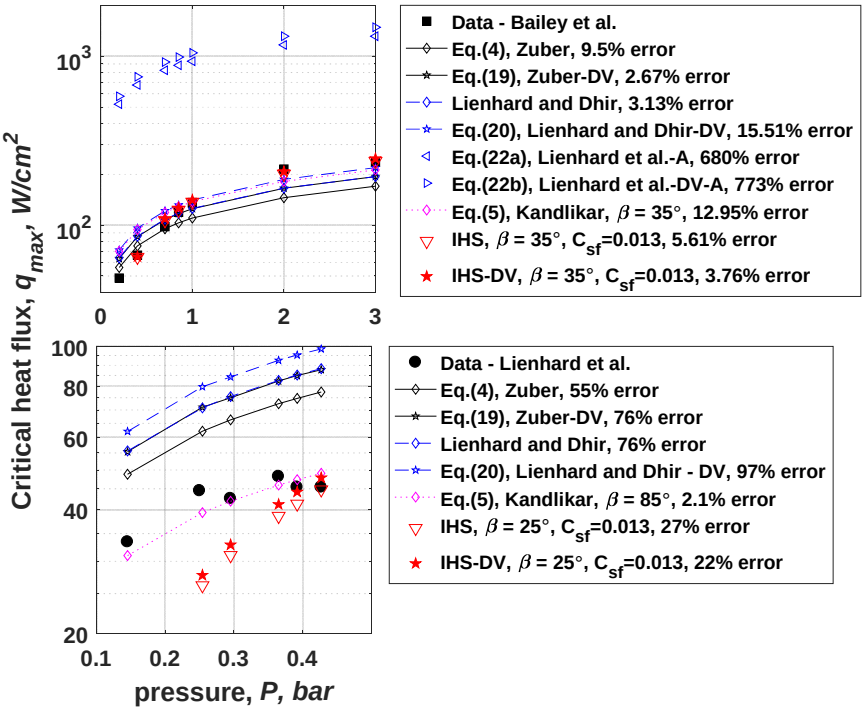

Fig. 5 The effect of pressure on the critical heat flux when boiling water. Percentage values on the legends are the average errors in predictions, and legends with "-DV" are corrected CHF models

Figure 5 also shows that the corrected Zuber model, and the original Lienhard and Dhir model fit reasonably well with the data reported by Bailey et al. but they overestimate the data reported by Lienhard et al. significantly. The model developed by Lienhard et al. to correct for the effect of heater size (i.e. Eq. (22)) also predicts a much higher CHF value compared to the experimental data.

Figure 6 shows the CHF results measured by Bailey *et al.* [18] and Lienhard *et al.* [28] when boiling methanol on a horizontal surface. It shows that all the model except for the original Zuber and IHS model can fit most of the experimental data reported by Bailey *et al.* within ±10% error. The best fitting data is the Kandlikar model and the revised Lienhard and Dhir model. When fitting the data reported by Lienhard *et al.*, all the model except for the corrected Zuber, the original and revised Lienhard and Dhir model result in less than 10% error on average. The best model is the original Zuber's model.

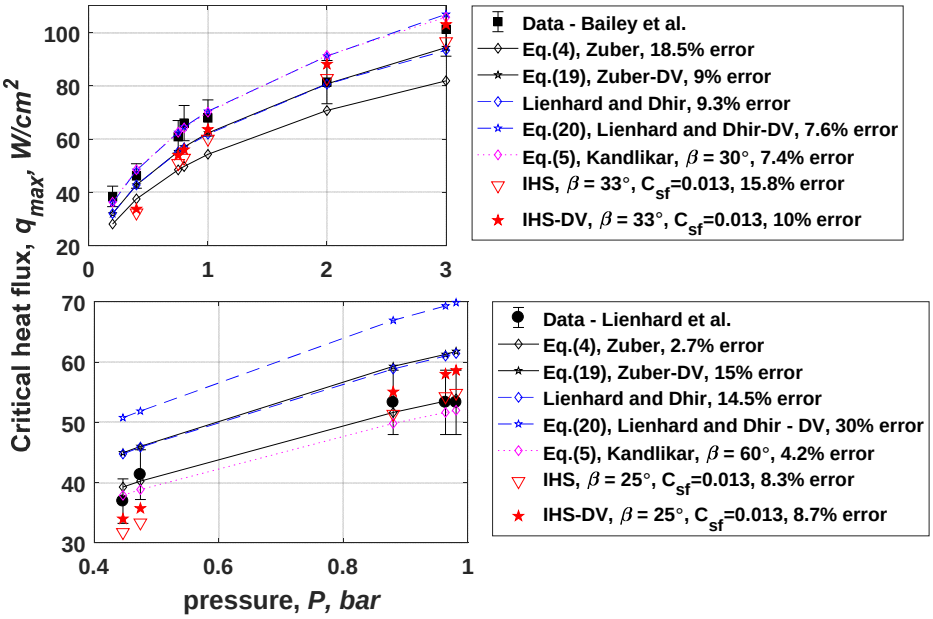

Fig. 6 The effect of pressure on the critical heat flux when boiling methanol. Error bars represent ±10% difference. Percentage values on the legends are the average errors in predictions, and legends with "-DV" are corrected CHF models

The CHF when boiling different types of cryogens has been experimentally investigated by Bewilogua *et al.* [29]. Comparison between their results of boiling helium and the CHF predicted by the CHF models is shown in Fig. 7. When using the IHS model, because there is no information about the C_{sf} found in existing literature, it is calculated by fitting the corrected IHS model to the data at 1 bar and assuming 5° contact angle. This extreme small contact angle also leads a very thick superheated microlayer where the nucleation can take place. Throughout the calculation, the superheated microlayer where the

nucleation takes place is assumed to be 10 μm. Figure 7 shows that although all the models can predict the shape of the CHF – Pressure curve well, the IHS model is the only model to be able to predict the CHF of boiling helium close to 95% accuracy on average. The second closest model is Kandlikar model with 0° contact angle and the average discrepancy between the predicted CHF and the measured one is 13% difference. The authors did not provide any contact angle information. The literature survey by Bald [31] concluded that the contact angle between the typical cryogens (e.g. liquid hydrogen, liquid nitrogen and liquid helium) and metal surface would be very small (< 10°) due to the much larger surface energy of the metal compared to that of cryogens. The corrections made to the Zuber model and Lienhard and Dhir model help to reduce the discrepancy between the predicted CHF and the measured ones. However, it is difficult to make a judgement on whether the corrected IHS model is more accurate than the original one because a smaller C_{sf} value can be used to increase the CHF predicted by the original IHS model.

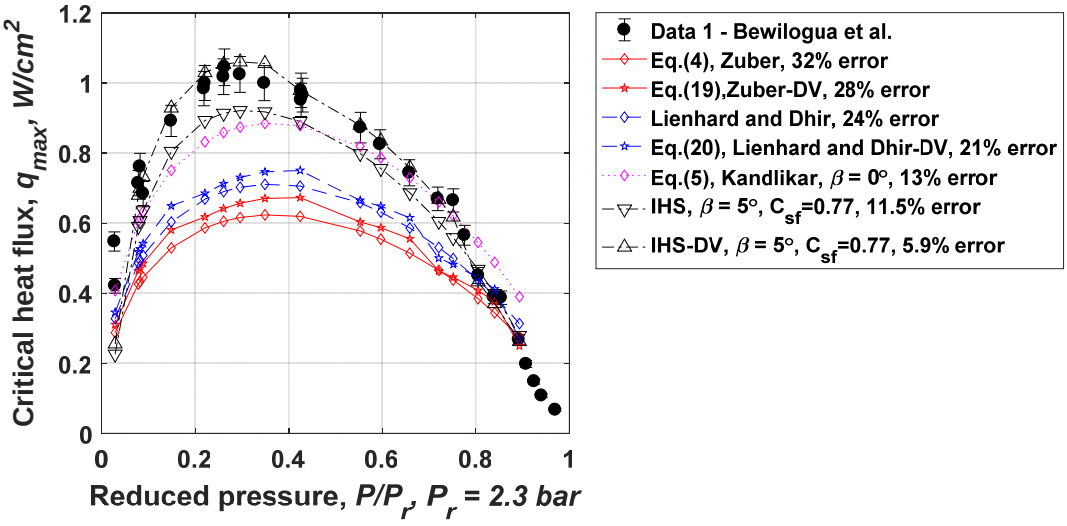

Fig. 7 The effect of pressure on the critical heat flux when boiling helium. Error bars represent ±5% difference. Percentage values on the legends are the average errors in predictions, and legends with "-DV" are corrected CHF models

The predicted and measured CHF value when boiling hydrogen is shown in Fig. 8. It shows that the Kandlikar model with 5° contact angle, and the corrected HIS model can predict the CHF within 10% error on average. Similar to the helium results, the corrected Lienhard and

Dhir model and the Zuber model can predict CHF more accurately. The CHF predicted by the corrected Lienhard and Dhir model is ~ 15% error on average.

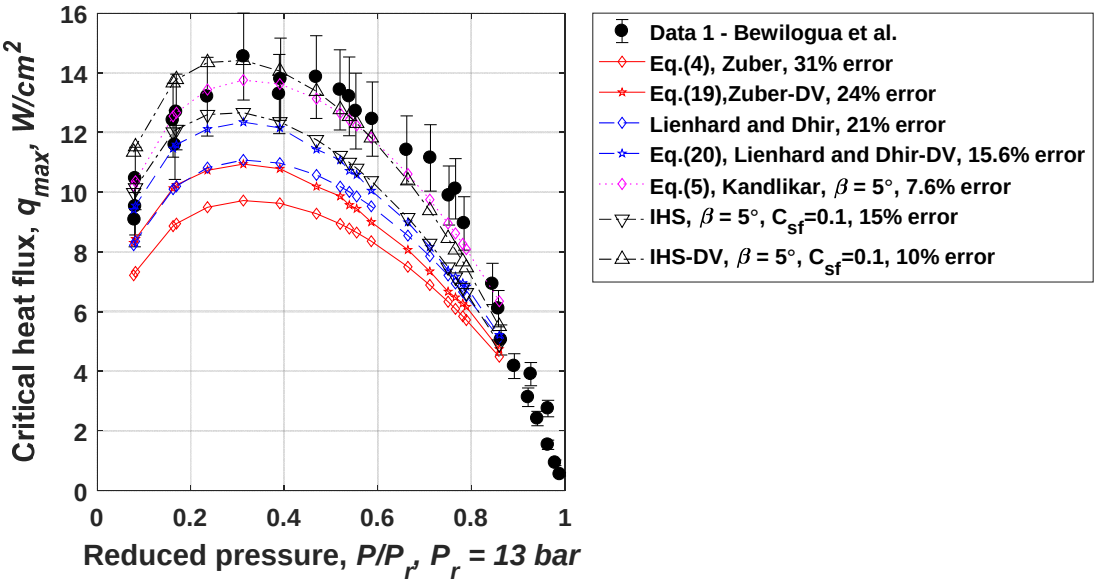

Fig. 8 The effect of pressure on the critical heat flux when boiling hydrogen. Error bars represent ±10% difference. Percentage values on the legends are the average errors in predictions, and legends with "-DV" are corrected CHF models

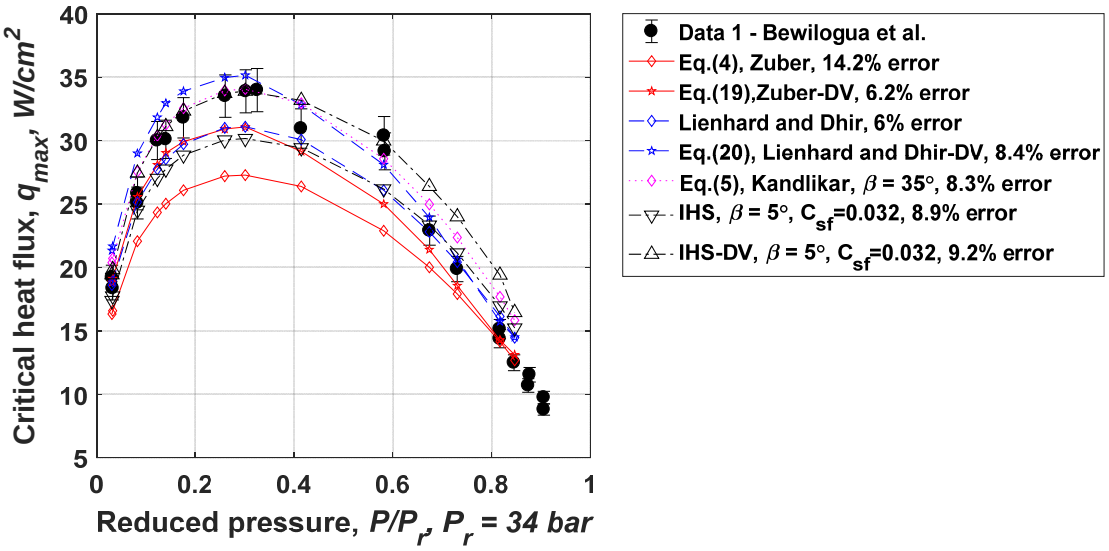

Fig. 9 The effect of pressure on the critical heat flux when boiling nitrogen. Error bars represent ±5% difference. Percentage values on the legends are the average errors in predictions, and legends with "-DV" are corrected CHF models

The predicted and measured CHF value when boiling nitrogen is shown in Fig. 9. It shows that all models except for the original Zuber model can predict the CHF within ±10% error on average.

In summary, the corrections made to the Zuber model, the Lienhard and Dhir model help to reduce their errors in predicting the CHF condition when boiling different types of cryogens. All the models can well predict the shape of the CHF – pressure curve. The existence of a maximum value of CHF is likely due to the competing effect of significantly reduced surface tension and the increased vapour density when the pressure increased. The reduced surface tension results in the less stable interface, so the required vapour velocity to induce the hydrodynamic instability is reduced. Meanwhile, the increased vapour density requires more mass of liquid to evaporate so a larger amount of heat will need to be absorbed.

5. Conclusion

Many of the most widely adopted CHF models are based on the hydrodynamic instability of the liquid-vapour interface, i.e. the Kelvin – Helmholtz (KH) instability. The KH theory used in these models are based on the analysis of the critical instability condition of a planar interface between two inviscid flow with infinite depths. However, in most boiling conditions, the interface of a vapour column is closer to a cylindrical surface, and the liquid phase always has noticeable viscosity. In addition, the literature suggested the vapour column mostly broke up in the most unstable condition instead of the critical instability condition. Therefore, to better match the actual physical process, the unstable condition predicted by the VCVPF theory has been applied to correct the existing CHF models. The comparison between the CHF conditions predicted by the existing models, the corrected models and the experimental data indicates the following significant findings:

1. The correction based on the unstable condition predicted by the VCVPF theory results in a higher CHF value in all cases. In addition, the corrected Zuber model predicts similar CHF value to the Lienhard and Dhir model.

2. The corrected IHS model can predict the effect of heater size on CHF marginally better than the original IHS model. These two models are much more accurate than all the other models, including the model developed by Lienhard *et al.* [28] which tends to overestimate the CHF values for a small heater.
3. The corrected Zuber model, the original Lienhard and Dhir model, together with the original and revised IHS models, can predict the effect of system pressure on water and methanol boiling CHF conditions within ±10% error when compared to the CHF measured by Bailey *et al.* [18]. However, they can lead to larger errors when compared to the water boiling CHF value reported by Lienhard et al. The Kandlikar model can well predict the CHF values on different pressure by choosing different values of contact angle. However, some of the contact angles, which lead to the best match, are much higher than the typical contact angle reported in the literature.
4. The corrections made to the Zuber model and the Lienhard and Dhir model consistently help to reduce the discrepancy between the predicted CHF and measured CHF when boiling different type of cryogens (e.g. liquid helium, liquid nitrogen and liquid hydrogen) across a wide pressure range. The IHS and the revised IHS models are the only models to be able to predict the CHF when boiling helium within ±5% error. The choice of the C_{sf} value and the correlation to predict the surface temperature needs further verification. The Kandlikar model can predict the CHF when boiling nitrogen and hydrogen with 10% on average. However, the contact angle leads to the best fit of nitrogen CHF-pressure curve in Kandlikar model is higher than the typical contact angle reported in the literature.

Nomenclature

A = area

C = constant

C_1 = bubble growth constant

C_p = heat capacity

g = gravitational acceleration

h = height

h_{lv} = enthalpy of evaporation

I_m = the modified Bessel function of the first kind

I'_m = the 1st order derivative of the modified Bessel function of the first kind

Ja = Jakob number

k = instability wavenumber (=$2\pi/\lambda$)

K_m = the modified Bessel function of the second kind

K'_m = the 1st order derivative of the modified Bessel function of the second kind

m = symmetry index (0 is for axisymmetric perturbation)

P = pressure

Pr = Prandtl number

q'' = heat flux

R = radius

S = distance

t = time

T = temperature

ΔT = excess temperature

U = uniform velocity

V = velocity

w_i = perturbation growth rate

Greek

α = heat and mass transfer coefficient in KH theory

α with subscript v or l = thermal diffusivity

β = contact angle

γ = bubble growth coefficient

δ = macrolayer thickness

λ = instability wavelength

μ = dynamic viscosity

ρ = density

σ = surface tension

τ = characteristic time

ϕ = surface inclination angle (0 for horizontal surface)

Subscripts

c = critical instability condition

CHF = critical heat flux condition

D = most unstable condition

g = bubble grow

HK = Haramura and Katto model

IHS = irreversible hot spot model

IPF = Inviscid potential flow analysis

K = Kandlikar model

KH = Kelvin-Helmholtz instability

l = liquid phase

L = length

LCB = large Coalescence bubble

LD = Lienhard and Dhir model

LD' = Corrected Lienhard and Dhir model

$neck$ = neck position in the merged bubble

NB = nuclei bubble

re = receding

RT = Rayleigh-Taylor instability

$PIPF$ = planar inviscid potential flow analysis

s = surface

sat = saturation condition

v = vapour phase

$VCVPF$ = Viscous correction for the viscous potential flow analysis

VPF = Viscous potential flow analysis

w = wait for bubble nucleation

Z = Zuber model

Z' = corrected Zuber model

References:

[1] Fang, X., and Dong, A., 2016, "A Comparative Study of Correlations of Critical Heat Flux of Pool Boiling," J. Nucl. Sci. Technol., **3131**(July), pp. 1–12.

[2] Zhao, H., and Williams, A., 2018, "Predicting the Critical Heat Flux in Pool Boiling Based on Hydrodynamic Instability Induced Irreversible Hot Spots," Int. J. Multiph. Flow.

[3] Carey, V. P., 2008, *Liquid-Vapor Phase Change Phenomena*, CRC Press.

[4] Funada, T., and Joseph, D. D., 2001, "Viscous Potential Flow Analysis of Kelvin–Helmholtz Instability in a Channel," J. Fluid Mech., **445**(May), pp. 263–283.

[5] Joseph, D. D., and Wang, J., 2004, "The Dissipation Approximation and Viscous Potential Flow," J. Fluid Mech., **505**, pp. 365–377.

[6] Awasthi, M. K., Asthana, R., and Agrawal, G. S., 2012, "Pressure Corrections for the Potential Flow Analysis of Kelvin–Helmholtz Instability with Heat and Mass Transfer," Int. J. Heat Mass Transf., **55**(9–10), pp. 2345–2352.

[7] Zhao, H., and Bhabra, B., 2018, "Experimental Investigation of the Kelvin-Helmholtz Instabilities of a Gas Column in Viscous Fluids," Int. J. Multiph. Flow.

[8] Kutateladze, S. S., 1950, "Hydromechanical Model of Heat Transfer Crisis in Pool Liquid Boiling," J. Tech. Phys., **20**(11).

[9] Zuber, N., 1959, "Hydrodynamic Aspects of Boiling Heat Transfer (Thesis)," United States At. Energy Commision, p. 196.

[10] Dhir, K., and Lienhard, H., 1973, *Extended Hydrodynamic Theory of the Peak and Minimum Pool Boiling Heat Fluxes*. NASA Contractor Report, NASA CR-2270.

[11] El-Genk, Mohamed S.; Guo, Z., 1993, "Transient Boiling from Inclined and Downward-Facing Surfaces in a Saturated Pool," Int. J. ref, **16**(6).

[12] Brusstar, Matthew J.; Merte, H., 1994, "Effects of Buoyancy on the Critical Heat Flux in Forced Convection," J. Thermophys. heat Transf., **8**(2).

[13] Kandlikar, S. G., 2001, "A Theoretical Model to Predict Pool Boiling CHF Incorporating Effects of Contact Angle and Orientation," J. Heat Transfer, **123**(6), p. 1071.

[14] Haramura, Y., and Katto, Y., 1983, "A New Hydrodynamic Model of Critical Heat Flux, Applicable Widely to Both Pool and Forced Convection Boiling on Submerged Bodies in Saturated Liquids," Int. J. Heat Mass Transf., **26**(3), pp. 389–399.

[15] Ahn, H. S., and Kim, M. H., 2012, "Visualization Study of Critical Heat Flux Mechanism on a Small and Horizontal Copper Heater," Int. J. Multiph. Flow, **41**, pp. 1–12.

[16] Chu, I. C., No, H. C., and Song, C. H., 2013, "Visualization of Boiling Structure and Critical Heat Flux Phenomenon for a Narrow Heating Surface in a Horizontal Pool of Saturated Water," Int. J. Heat Mass Transf., **62**(1), pp. 142–152.

[17] Chu, I. C., No, H. C., Song, C. H., and Euh, D. J., 2014, "Observation of Critical Heat Flux Mechanism in Horizontal Pool Boiling of Saturated Water," Nucl. Eng. Des., **279**, pp. 189–199.

[18] Bailey, W., Young, E., Beduz, C., and Yang, Y., 2006, "Pool Boiling Study on

Candidature of Pentane, Methanol and Water for near Room Temperature Cooling," *Thermal and Thermomechanical Proceedings 10th Intersociety Conference on Phenomena in Electronics Systems, 2006. ITHERM 2006.*, IEEE, pp. 599–603.
[19] Rohsenow, W. M., 1951, "A Method of Correlating Heat Transfer Data for Surface Boiling of Liquids," J. Heat Transfer, **74**, pp. 969–976.
[20] Sakashita, H., Ono, A., and Nakabayashi, Y., 2010, "Measurements of Critical Heat Flux and Liquid-Vapor Structure near the Heating Surface in Pool Boiling of 2-Propanol/water Mixtures," Int. J. Heat Mass Transf., **53**(7–8), pp. 1554–1562.
[21] Wiebe, J. R., and Judd, R. L., 1971, "Superheat Layer Thickness Measurements in Saturated and Subcooled Nucleate Boiling," J. Heat Transfer, **93**(4), p. 455.
[22] Davis, E. J., and Anderson, G. H., 1966, "The Incipience of Nucleate Boiling in Forced Convection Flow," AIChE J., **12**(4), pp. 774–780.
[23] Asthana, R., Awasthi, M. K., Agrawal, G. S. S., Asthana, R., Agrawal, G. S. S., Awasthi, M. K., and Agrawal, G. S. S., 2014, "Viscous Correction for the Viscous Potential Flow Analysis of Kelvin-Helmholtz Instability of Cylindrical Flow with Heat and Mass Transfer," Int. J. Heat Mass Transf., **43**(6), pp. 251–259.
[24] Lee, D.-S., 2007, "Nonlinear Kelvin–Helmholtz Instability of Cylindrical Flow with Mass and Heat Transfer," Phys. Scr., **76**(1), pp. 97–103.
[25] Funada, T., and Joseph, D. D., 2002, "Viscous Potential Flow Analysis of Capillary Instability," Int. J. Multiph. Flow, **28**(9), pp. 1459–1478.
[26] Awasthi, M. K., and Agrwal, G. S., 2011, "Viscous Potential Flow Analysis of Kelvin-Helmholtz Instability of Cylindrical Interface," Int. J. Appl. Math. Comput., **3**(2), pp. 131–140.
[27] Wang, J., Joseph, D. D., and Funada, T., 2005, "Viscous Contributions to the Pressure for Potential Flow Analysis of Capillary Instability of Two Viscous Fluids," J. Fluid Mech., **522**, pp. 383–394.
[28] Lienhard, H., Dhir, V. K., and Riherd, D., 1973, "Peak Pool Boiling Heat -Flux Measurements on Finite Horizontal Flat Plates," J. Heat Transfer, (November), pp. 477–482.
[29] Bewilogua, L., Knöner, R., and Vinzelberg, H., 1975, "Heat Transfer in Cryogenic Liquids under Pressure," Cryogenics (Guildf)., **15**(3), pp. 121–125.
[30] Horsthemke, A., and J. J., S., 1985, "The Wettability of Industrial Surfaces : Contact Angle Measurements and Thermodynamic Analysis *," Chem. Eng. Process., **19**, pp. 277–285.
[31] Bald, W. B., 1973, "Cryogenic Heat Transfer Research at Oxford. Part 1 - Nucleate Pool Boiling," Cryogenics (Guildf)., **13**(8), pp. 457–469.

List of figures:

List of Tables: